ELSEVIER

Journal of Power Sources 110 (2002) 201–208

JOURNAL OF POWER SOURCES

www.elsevier.com/locate/jpowsour

Electrode behaviour at (La,Sr)MnO_3/Y_2O_3–ZrO_2 interface by electrochemical impedance spectroscopy

S.P. Jiang[a,*], J.G. Love[b], Y. Ramprakash[b]

[a]*Fuel Cells Strategic Research Program, School of Mechanical and Production Engineering, Nanyang Technological University, Nanyang Avenue, Singapore 639798, Singapore*

[b]*Ceramic Fuel Cells Limited, 170 Browns Road, Noble Park, Vic. 3174, Australia*

Received 3 February 2002; accepted 24 April 2002

Abstract

The electrode behaviour of strontium (Sr)-doped $LaMnO_3$ (LSM) electrodes is investigated by an electrochemical impedance spectroscopy technique over the temperature range 850–1000 °C and the oxygen partial pressure range 0.01–0.21 atm. The electrodes are screen-printed on 50 mm × 50 mm 3 mol% Y_2O_3–ZrO_2 electrolyte cells with an electrode surface area of 10 cm^2. The impedance responses show two separable arcs and are analysed in terms of two different equivalent circuits with comparable information on the electrode processes at high and low frequencies. The electrode process associated with the high-frequency arc is essentially independent of O_2 partial pressure with an activation energy of ~74 kJ mol^{-1}, while that at the low-frequency arc has an activation energy of ~202 kJ mol^{-1} and a reaction order with respect to O_2 partial pressure of ~0.5 at low temperatures and ~0.85 at high temperatures. The electrode processes associated with the low- and high-frequency arcs are discussed.

Keywords: Electrochemical impedance; LSM cathodes; Solid oxide fuel cell; Oxygen reduction

1. Introduction

Strontium-doped $LaMnO_3$ (LSM) is the most common electrode (cathode) material for O_2 reduction reaction in solid oxide fuel cells (SOFCs) [1–3]. The kinetic behaviour and electrochemical mechanism of the oxygen reduction reaction at the LSM/Y_2O_3–ZrO_2 (YSZ) interface is therefore important for the development of SOFCs and has been extensively investigated by electrochemical impedance spectroscopy (EIS). In most cases, the impedance response for O_2 reduction at the LSM/YSZ interface is characterised by two depressed arcs and has been analysed using equivalent circuits [4–7]. Reaction time constant which range from one [8,9], two [4,10], three [11–13] and four [14] has been disclosed.

Despite the large number of EIS studies reported in the literature, there is no conclusive interpretation of the impedance response of O_2 reduction at the LSM/YSZ interface. The rate-determining step has been attributed to either an oxygen dissociative adsorption process [4,5], gas-phase O_2 diffusion [7,9] or oxygen diffusion on the LSM surface [10,12,15]. Brichzin et al. [16] and Kuznecov et al. [17] also proposed that O_2 reduction could be associated with oxygen diffusion through the LSM bulk. The discrepancies in the literature with regard to the actual mechanism of the O_2 reduction at LSM/YSZ interfaces may be intrinsically linked to variability in LSM/YSZ microstructure, morphology of LSM particles, and cathodic current treatment of the cathode. For example, the initial impedance behaviour for O_2 reduction on LSM electrodes is strongly affected by cathodic current treatment [6,12]. Depending on the conditions of this treatment, namely, current density, temperature and polarisation period, the impedance behaviour can be characterised with between one and three arcs [12]. This behaviour has been attributed to changes in microstructure in the LSM and the YSZ interface region [18]. A recent study has shown [19] that the initially very high polarisation losses and electrode resistance can also originate from the presence of passivation species such as MnO_x and in particular, SrO which is originally enriched on the LSM surface. Cathodic polarisation is effective in removing or decreasing the concentration of the passivation species at the reaction sites close to the three-phase boundary region.

In this work, O_2 reduction on porous LSM electrodes studied by means of electrochemical impedance spectroscopy on 50 mm × 50 mm electrolyte cells with an electrode surface area of 10 cm^2 under fuel cell operation conditions.

* Corresponding author. Tel.: +65-6790-5010; fax: +65-6791-1859.
E-mail address: mspjiang@ntu.edu.sg (S.P. Jiang).

0378-7753/02/$ – see front matter
PII: S0378-7753(02)00259-8

The large electrode surface area is typical for solid electrolyte cells used to evaluate the performance and long-term stability evaluation under SOFC operation conditions [20]. The impedance was measure as a function of temperature (850–1000 °C) and oxygen partial pressure (0.21–0.01 atm) under open-circuit potential (OCP) conditions and was characterised by equivalent-circuit analysis.

2. Experimental

Strontium-doped lanthanum manganite with a composition of $(La_{0.82}Sr_{0.18})_{0.82}MnO_3$ (LSM) was prepared by a co-precipitation method followed by coarsening at 1000 °C. The A-site non-stoichiometric composition of LSM is effective in inhibiting the formation of the insulating lanthanum zirconate phase [12]. The powder was prepared into electrode ink and screen-printed on to 50 mm × 50 mm electrolyte plates of 3 mol% Y_2O_3–ZrO_2 (TZ3Y, Tosoh, Japan). The electrolyte plate was prepared by tape casting and fired at 1500 °C. The thickness of the sintered plate was ∼195 μm. The anode was a conventional Ni/TZ3Y cermet with a volume percentage of 50/50 and was screen-printed on to the opposite side of the TZ3Y electrolyte plate. The Ni/TZ3Y cermet anode and LSM cathode were fired separately in air at 1400 and 1150 °C, respectively. The area of the LSM cathode and the Ni/TZ3Y anode was 10 cm^2. Long strips of LSM and Ni/TZ3Y were also screen-printed on the cathode and the anode sides, respectively, to serve as reference electrodes. The impedance behaviour of the LSM electrode was measured against the anode side Ni/TZ3Y strip reference electrode. Ni and Pt meshes were used as current-collectors on the anode and the cathode side, respectively. Separate Pt voltage probes were provided for the electrochemical measurements. The fuel composition at the anode side was kept constant at 96% H_2/4% H_2O. The air and fuel flow rates were 2 l min^{-1}. The gas was directed on to the centre of the electrodes and distributed evenly across the electrode area through distribution channels in alumina blocks. The fuel electrode side was sealed with a high temperature gasket. The cell configuration and the gas flow direction are shown in Fig. 1.

In the measurements, the cell was heated to 1000 °C and the electrode behaviour of the LSM cathode was stabilised by polarisation with a current density of 250 mA cm^{-2} for more than 100 h. Then, the impedance measurements were performed using a Voltech TF2000 frequency response analyser in conjunction with a potentiostat (Utah Electronics, model 0152) over the frequency range from 100 kHz to 1 Hz with an amplitude of 14 mV. The measurements were performed first at 1000 °C and changing the O_2 partial pressure (P_{O_2}) from 0.21, 0.10, 0.05 to 0.01 atm (high purity pre-mixed O_2/N_2, CIG, Australia), and then subsequently at 950, 900 and finally at 850 °C. The composition of the gas mixture was also checked from the open-circuit potential measured against fuel gas of 96% H_2/4% H_2O. The impedance curves were analysed by a non-linear least squares (NLLS) analysis program developed by Boukamp [21].

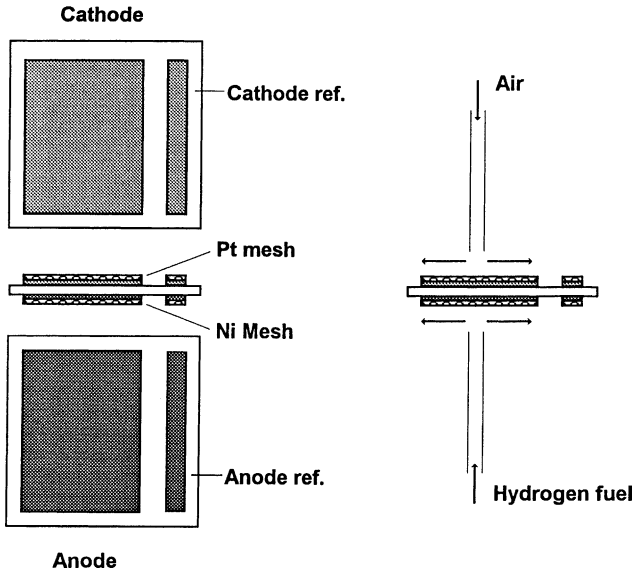

Fig. 1. Schematic diagram of cell configuration.

3. Results

The impedance responses measured at open-circuit at temperatures between 850 and 1000 °C and P_{O_2} between 0.01 and 0.21 atm are presented in Fig. 2. The responses are generally characterised by overlapping and depressed arcs. At low P_{O_2} and low temperatures, the arcs became clearly separated at low and high frequencies. This indicates that at least two electrochemical processes contribute to the overall electrochemical reaction. The electrode impedance responses at high frequencies appears to be independent of oxygen partial pressure at all temperatures, while those at low frequencies, show a significant dependence on the oxygen partial pressure. The magnitude of both arcs changes significantly with the temperature.

For the impedance responses shown in Fig. 2, three different equivalent circuits have been used for the fitting, as shown in Fig. 3. In the circuits, L is the inductance, R_Ω the ohmic resistance of the electrode measured between the cathode and the anode reference electrodes R_1 and R_2 the electrode interface (polarisation) resistance at high and low frequencies, CPE1 and CPE2 the corresponding constant-phase elements (referred to as Q in Boukamp's NLLS analysis program [21]), and W_R the R-type diffusion impedance. The inductance component (L) observed at high frequencies is found to be ∼11 μH from the NLLS fitting and is relatively constant over the experimental conditions studied. The high-frequency intercept of the impedance spectra is attributed to the ohmic resistance between the LSM cathode and the anode reference electrode (R_Ω in the equivalent-circuit). The first equivalent-circuit (Fig. 3(a)) of

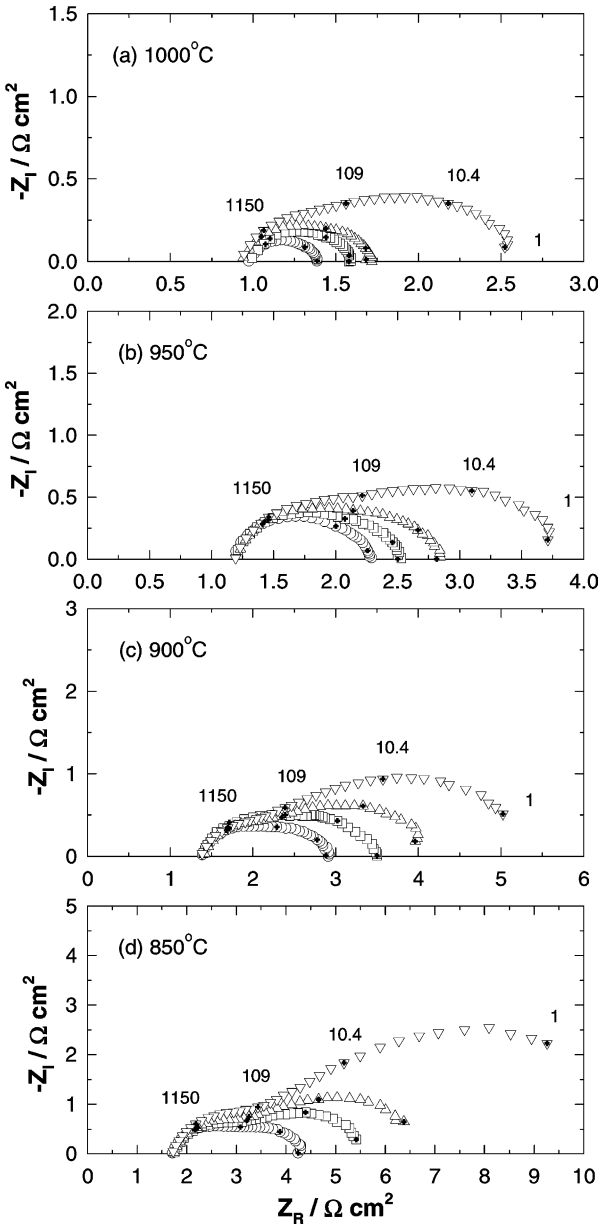

Fig. 2. Impedance responses measured at (a) 1000 °C, (b) 950 °C, (c) 900 °C and (d) 850 °C at different partial pressure of O_2: (○) 0.21 atm, (□) 0.10 atm, (△) 0.05 atm, (▽) 0.01 atm. Numbers in the figure are frequencies in Hz.

two R-CPE circuits in series (series RC) describes two rate-limiting electrode processes in series. The second circuit (Fig. 3(b)) is a nested or ladder type of two R-CPE circuits (nested RC), which is generally used to describe two inter-related limiting electrode processes such as the mass-transport controlled charge-transfer processes. The third circuit (Fig. 3(c)) represents R-type diffusion impedance and has been observed for O_2 reduction at a very low partial pressure of oxygen in a solid oxide electrochemical system [22].

The selected circuits have been used to fit the observed impedance responses. An example of the fitting for the impedance responses measured at 850 °C and $P_{O_2} = 0.01$ atm, is

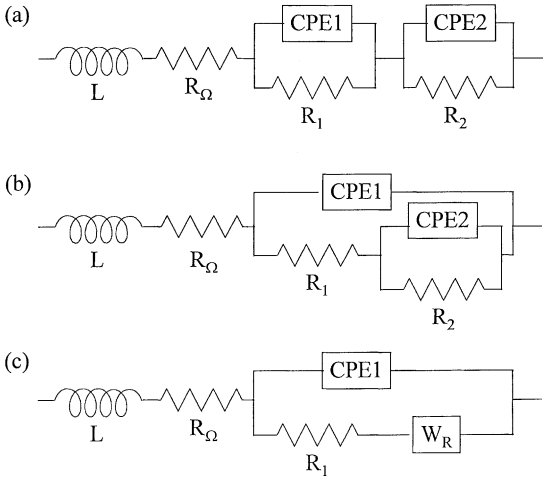

Fig. 3. Equivalent circuits used for fitting: (a) series RC, (b) nested RC, (c) R-type impedance.

shown in Fig. 4. The fittings between the experimental and the calculated data are generally good except at low frequencies where the calculated data start to deviate from the measured values. The difference between the fitted real and imaginary impedance data and the experimental ones measured at 850 °C and $P_{O_2} = 0.01$ atm is shown in Fig. 5 as a function of the sampling frequency. The large deviation indicates poor fitting of the equivalent circuits to the observed impedance patterns. The best fit is found for the equivalent circuits of series RC (Fig. 3(a)) and nested RC (Fig. 3(b)). Over the entire temperature and P_{O_2} ranges investigated, the series RC and nested RC circuits give overall good fits, while the fitting of the R-type equivalent-circuit is much poorer especially with experimental data at high temperatures and high P_{O_2}. The reason for the poor fit of the R-type circuit is probably related to the constant frequency exponent of 0.5 in the R-type impedance. This would yield a partial arc at low frequencies centred on the real impedance axis. The observed depressed low-frequency arcs indicate that the frequency exponent for R-type impedance would have to deviate from 0.5 to provide a good fit [16]. The physical reason for having an exponent other than

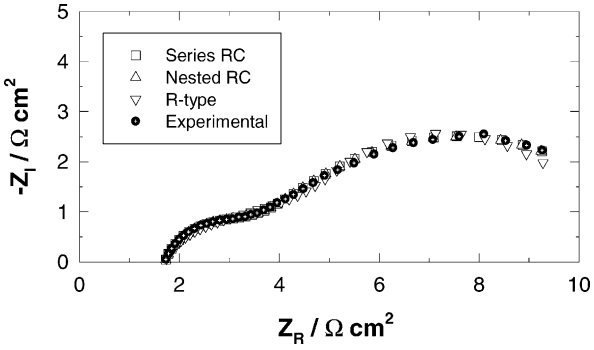

Fig. 4. Fitting of various equivalent circuits, as shown in Fig. 3, to experimental data (●) measured at 850 °C and O_2 partial pressure of 0.01 atm.

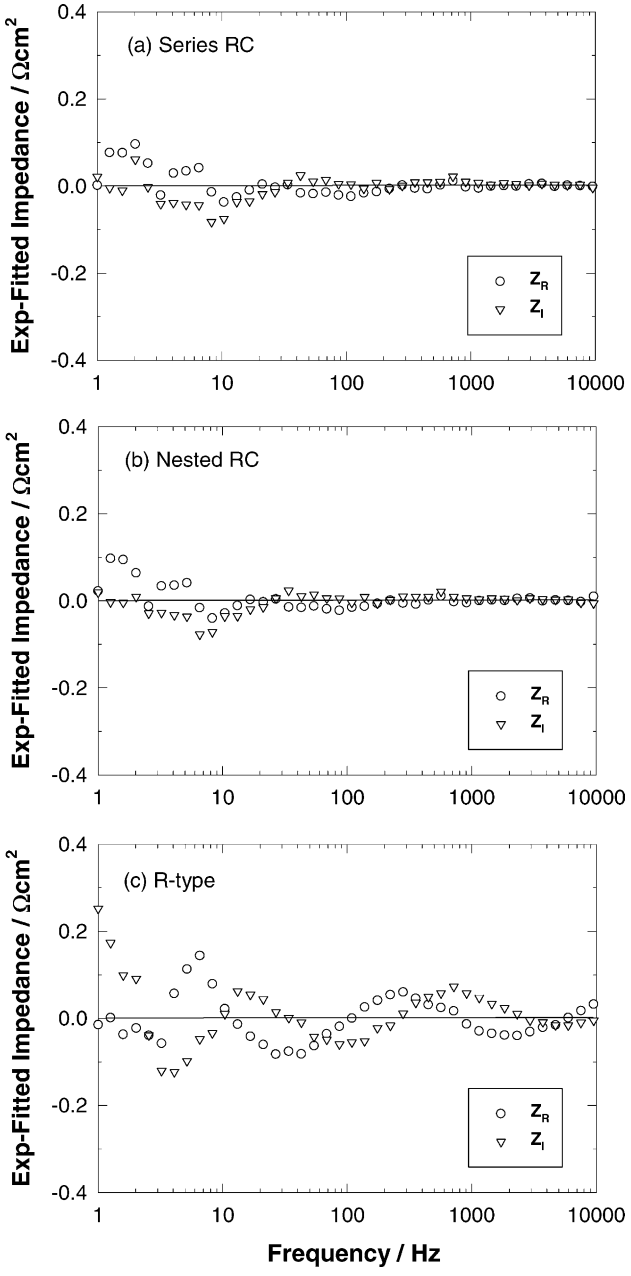

Fig. 5. (a–c) Deviation of equivalent-circuit fittings to measured data for real (○) and imaginary (▽) impedance. Experimental data measured at 850 °C and O_2 partial pressure of 0.01 atm.

0.5 for R-type impedance is not clear at this stage. Therefore, the series RC and nested RC circuits were chosen for analysis of the O_2 reduction reaction on the screen-printed LSM electrodes (see following sections).

Arrhenius plots for the electrode interface conductivity (σ is reciprocal of electrode interface resistance) of high- and low-frequency arcs ($\sigma_1 = 1/R_1$ and $\sigma_2 = 1/R_2$) are shown in Fig. 6 for different P_{O_2} obtained from the NLLS fit of the series RC circuit. Results for the nested RC circuit are given in Fig. 7. Activation energies calculated from the slopes of the Arrhenius plots are given in Table 1 for the two circuits at different P_{O_2}. As shown in Figs. 6(a) and 7(a), the electrode

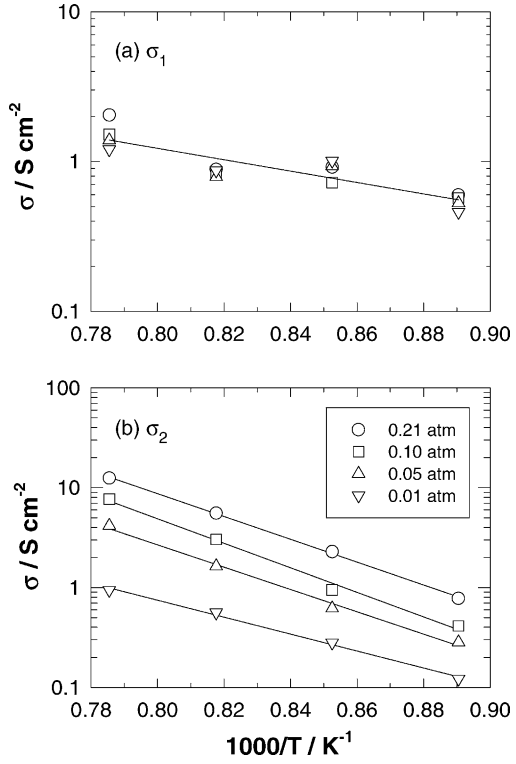

Fig. 6. Arrhenius plots for (a) σ_1 and (b) σ_2 determined from NLLS analysis of series RC circuit at different partial pressures of O_2. Line is best fit from regression analysis.

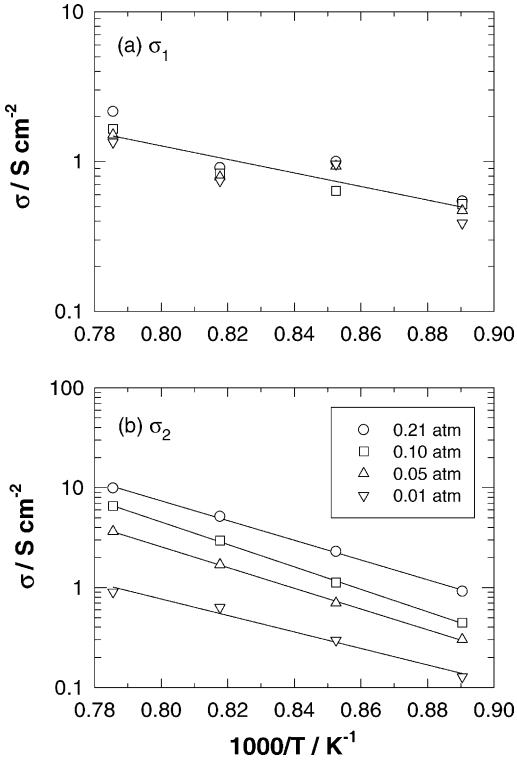

Fig. 7. Arrhenius plots for (a) σ_1 and (b) σ_2 determined from NLLS analysis of nested RC circuit at different partial pressures of O_2. Line is best fit from regression analysis.

Table 1
Activation energy of σ_1 and σ_2 evaluated using series RC and nested RC equivalent circuits at different partial pressures of oxygen

P_{O_2} (atm)	Activation energy, E_a (kJ mol^{-1})			
	Series RC circuit		Nested RC circuit	
	σ_1	σ_2	σ_1	σ_2
0.21	86	219	68	198
0.10	72	236	68	222
0.05	59	214	78	206
0.01	65	163	95	158
Average	71 ± 11	208 ± 31	77 ± 12	196 ± 27

conductivity of the high-frequency arc (σ_1) is not affected by the partial pressure of O_2. On average, the activation energy of the high-frequency arc, σ_1 is 71 ± 11 kJ mol^{-1} for the series RC circuit and 77 ± 12 kJ mol^{-1} for the nested RC circuit. This indicates that the electrode process associated with the high-frequency arc is essentially independent of P_{O_2}. The electrode process associated with the low-frequency arc is strongly affected by P_{O_2}, namely, the higher P_{O_2}, the higher σ_2 for O_2 reduction. The activation energy of the electrode process associated with the low-frequency arc appears, however, to be independent of P_{O_2}. The activation energy of the electrode conductivity of the low-frequency arc (σ_2) is 208 ± 31 kJ mol^{-1} for the series RC circuit and 196 ± 27 kJ mol^{-1} for the nested RC circuit.

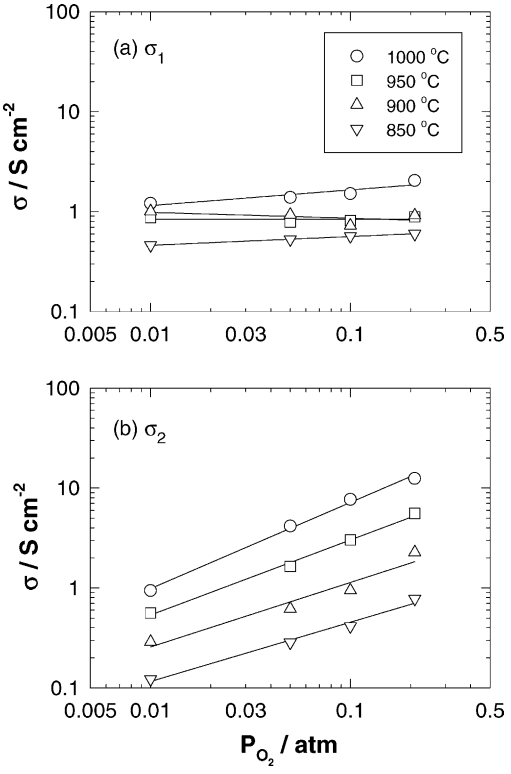

Fig. 8. Plots of log σ–log P_{O_2} for (a) σ_1 and (b) σ_2 determined from NLLS analysis of series RC circuit at different temperatures. Line is best fit from regression analysis.

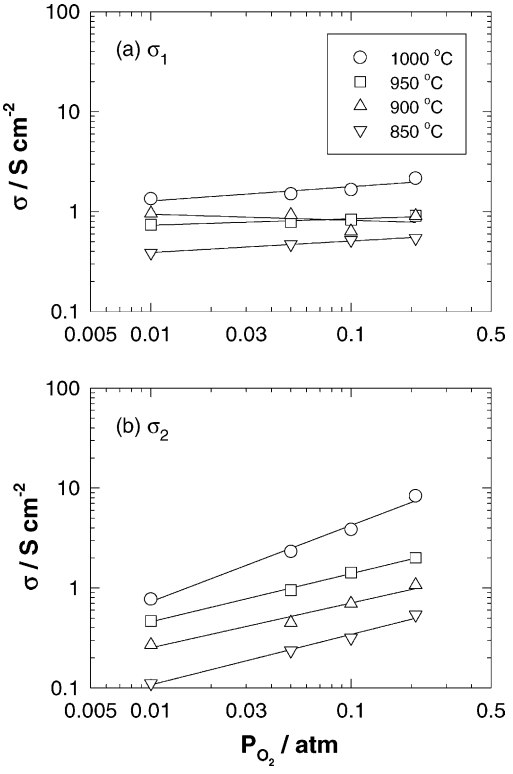

Fig. 9. Plots of log σ–log P_{O_2} plots for (a) σ_1 and (b) σ_2 determined from NLLS analysis of nested RC circuit at different temperatures. Line is best fit from regression analysis.

The P_{O_2} dependence of the electrode conductivity for the low- and high-frequency arcs was determined from the log σ–log P_{O_2} plots at different temperatures for the series RC circuit (Fig. 8) and nested RC circuit (Fig. 9). The reaction orders with respect to P_{O_2} determined from the slope at different temperatures are listed in Table 2. As shown, the reaction order with respect to P_{O_2} for the electrode reaction at the high-frequency arc (σ_1) is close to zero (0.05 ± 0.1 on average) and is almost independent of temperature. For the electrode reaction at the low-frequency arc (σ_2), however, the reaction order appears to be related to the temperature and decreases with decreasing temperature. For the series RC circuit, the reaction order with respect to P_{O_2} is 0.86 at 1000 °C and 0.59 at 850 °C. For the nested RC circuit, the

Table 2
Reaction order with respect to P_{O_2} for σ_1 and σ_2 evaluated using series RC and nested RC equivalent circuits at different temperatures

Temperature (°C)	Reaction order, x in $P_{O_2}^x$			
	Series RC circuit		Nested RC circuit	
	σ_1	σ_2	σ_1	σ_2
1000	0.15	0.86	0.14	0.76
950	0	0.75	0.06	0.48
900	−0.05	0.64	−0.06	0.45
850	0.08	0.59	0.11	0.50

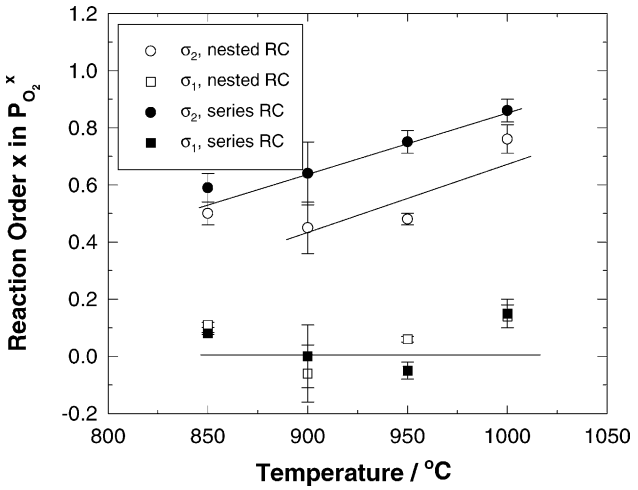

Fig. 10. Comparison of reaction order with respect to P_{O_2} of σ_1 and σ_2 for series RC (open symbols) and nested RC (filled symbols) as function of temperature. Error bars were obtained from regression analysis and lines are for guide only.

reaction order is 0.75 at 1000 °C and decreases to 0.45 for temperatures below 1000 °C. The series RC circuit gives overall higher reaction orders for σ_2 than those from the nested RC circuit. The temperature dependence of the reaction order with respect to the partial pressure of oxygen is summarised in Fig. 10. In general, the reaction order for the electrode process associated with the low-frequency arc decreases with decrease in temperature.

The exponent n in $(j\omega)^{-n}$ for the CPE components is found to be ~0.7 when determined from the NLLS analysis for both equivalent circuits. The value of CPE1 is around 2 ± 1 mF cm^{-2} for both the series RC and the nested RC circuits and is relatively independent of P_{O_2}. The value of CPE2 ranges from 18 to 32 mF cm^{-2} and appears to have a complex dependence on P_{O_2} and temperature. In general, capacitance value of high- and low-frequency arcs is consistent with those measured on porous LSM electrodes with much smaller electrode area (0.44 cm^2) [13]. Large errors in CPE1 and CPE2 determined from the NLLS fit routine prevent more exact analysis.

4. Discussion

The fitting of the series RC and nested RC equivalent circuits to the observed impedance data shows only a subtle difference within the relative errors of the NLLS fitting program. Therefore, both equivalent circuits could be applicable to the electrochemical processes of the O_2 reduction reaction based purely on the overall fitting of the impedance responses. This, in turn, indicates the difficulties in the application and interpretation of equivalent-circuit fittings as there is not a one-to-one correspondence between the equivalent-circuit and the impedance pattern. The observed separable two impedance arcs at low and high frequencies show, however, that the O_2 reduction reaction is at least limited by two electrode processes.

The activation energy of the electrode process at the low-frequency arc (158–236 kJ mol^{-1}) agrees with that reported by Youngblood et al. [4] for a pressed LSM electrode and by the present authors for a porous LSM electrode with a much smaller electrode area (0.44 cm^2) [13]. The capacitance value of the low-frequency arc is in the range 18–32 mF cm^{-2}, which is consistent with the high pseudo-capacitance values usually associated with adsorption and diffusion processes as observed for H_2 adsorption and diffusion on Ni surface at Ni/YSZ cermet anodes [23] and for surface adsorption of oxygen on a Pt electrode [24]. The reaction order with respect to the partial pressure of oxygen in the present study is in the range 0.45–0.86 and generally decreases with decreasing temperature (Fig. 10). As shown by Takeda et al. [25], a reaction order of 0.5 with respect to the partial pressure of oxygen indicates a reaction limited by the atomic oxygen concentration, whereas a value of 1 indicates a reaction limited by molecular oxygen concentration. This suggests that the electrode process at the low-frequency arc is most likely a mixed process of dissociative adsorption and diffusion limited by atomic oxygen and molecular oxygen concentration. The change in reaction order with respect to P_{O_2} may be due to the fact that the relative magnitude of the reaction rates of adsorption and diffusion of oxygen on the LSM surface could be influenced by temperature. The results of this study are generally in agreement with the common consensus that the electrode processes at low frequencies are related to the dissociative adsorption and diffusion of oxygen on the LSM surface [4,7,13] The activation energy of σ_2 (ranging from 158 to 236 kJ mol^{-1}) is close to that of oxygen trace diffusion (250–300 kJ mol^{-1}) [26], which indicates that the adsorption and surface diffusion processes associated with the low-frequency arc may proceed through an oxygen-vacancy transportation mechanism at the LSM surface.

The electrode process associated with the high-frequency arc are characterised by an activation energy of ~70 kJ mol^{-1} and a zero reaction order with respect to the partial pressure of oxygen. The capacitance of the high-frequency arc is in the range 2 ± 1 mF cm^{-2}. On a porous LSM electrode with an electrode area of 0.44 cm^2 the capacitance of the high-frequency arc is found to be between 3.4 and 20 mF cm^{-2} [13]. In another study, van Heuveln et al. [6] reported the capacitance of the high-frequency arc to be as high as 1 mF cm^{-2} for LSM cathodes with 60% contact to the YSZ surface. These workers attributed this capacitance to the double-layer capacitance of the LSM/electrolyte interface. This capacitance value appears, however to be too high to be associated with a double-layer capacitance. A recent investigation of O_2 reduction on porous LSM electrodes showed that the electrode conductivity of the high-frequency arc (σ_1) is basically independent of the dc bias [27]. This indicates that the electrode process at high frequencies cannot be associated with a charge-transfer process. The impedance of the high-frequency arc has an

activation energy close to that for oxygen ionic conduction in YSZ materials [28]. All these observations suggest that the electrode process associated with the high-frequency arc may be the migration and diffusion of oxygen ions from the three-phase boundary into zirconia electrolyte lattice. The observed independence of σ_1 with oxygen partial pressure indicates that the migration and diffusion of oxygen ions into zirconia electrolyte may be primarily limited by the oxygen ion conductivity of the electrolyte as the oxygen ion conductivity of YSZ is not affected by the P_{O_2} under the conditions studied [29]. This is also supported by the report [30] that the exchange current density of cathodes for oxygen reduction increases with the ionic conductivity of the electrolyte. The association of the high-frequency arc with the presence of $La_2Zr_2O_7$ at the electrode/electrolyte interface [31] may not be possible in the present study as the excess manganese in the A-site non-stoichiometry LSM composition would inhibit the $La_2Zr_2O_7$ formation [32].

As shown in the present study and by others [16], there is not a one-to-one correspondence between the equivalent-circuit and electrode reaction process. Thus, equivalent analysis of electrode impedance alone is not able to distinguish the oxygen diffusion reaction dominated by the surface or the bulk diffusion path for the O_2 reduction on LSM electrodes. On the other hand, an independent and detailed study of O_2 reduction on porous LSM electrodes with introduction of surface diffusion inhibiting species (i.e. gaseous Cr species) have provided clear evidence that O_2 reduction is dominated by surface processes related to dissociative adsorption and diffusion of oxygen on the LSM surface [13,27].

5. Conclusions

Impedance responses of O_2 reduction on the LSM/YSZ interface of a 50 mm × 50 mm fuel cell at open-circuit shows two arcs over the temperature range 850–1000 °C and the oxygen partial pressure range 0.01–0.21 atm. These arcs fitted by NLLS for two different equivalent circuits, namely, the series RC and the nested RC circuits. Both show good fit over the full experimental range with compatible electrode process information. The high-frequency arc can be attributed to the migration and diffusion of oxygen species from the three-phase boundary region into the zirconia electrolyte and has some characteristics of electrolyte contribution. It is essentially independent of oxygen partial pressure with an activation energy of around 74 kJ mol^{-1}. The activation energy of the reaction associated with low-frequency arc is ∼202 kJ mol^{-1} and has a reaction order with respect to oxygen partial pressure of 0.5 at low temperatures and ∼0.86 at high temperatures. The electrode processes at the low-frequency arc can be attributed to concentration impedance associated with dissociative adsorption and diffusion of oxygen on the LSM surface. This study shows that the electrode impedance behaviour on large electrolyte cells (10 cm^2) is essentially the same as that reported on the electrolyte cells with much smaller areas (e.g. 0.44 cm^2 or smaller) [4,13].

Acknowledgements

The authors thank members of the fabrication group of Ceramic Fuel Cells Limited for the supply of 50 mm × 50 mm electrolyte cells.

References

[1] N.Q. Minh, J. Am. Ceram. Soc. 76 (1993) 563.
[2] H. Yokokawa, N. Skai, T. Horita, K. Yamaji, Fuel Cells 1 (2001) 117.
[3] S.P.S. Badwal, K. Foger, Mater. Forum 21 (1997) 183.
[4] G.E. Youngblood, A.S. Rupaal, L.R. Pederson, J.L. Bates, in: S.C. Singhal, H. Iwahara (Eds.), Solid Oxide Fuel Cells III, The Electrochemical Society, Pennington, NJ, 1993, p. 585.
[5] B. Gharbage, T. Pagnier, A. Hammou, J. Electrochem. Soc. 141 (1994) 2118.
[6] F.H. van Heuveln, H.J.M. Bouwmeester, J. Electrochem. Soc. 144 (1997) 134.
[7] K. Tsuneyoshi, K. Mori, A. Sawata, J. Mizusaki, H. Tagawa, Solid State Ionics 35 (1989) 263.
[8] E. Siebert, A. Hammouche, M. Kleitz, Electrochim. Acta 40 (1995) 1741.
[9] J. van Herle, A.J. McEvoy, K.R. Thampi, Electrochim. Acta 41 (1996) 1447.
[10] Y. Matsuzaki, I. Yasuda, Solid State Ionics 126 (1999) 307.
[11] M.J.L. Østergård, M. Mogensen, Electrochim. Acta 38 (1993) 2015.
[12] S.P. Jiang, J.G. Love, J.P. Zhang, M. Hoang, Y. Ramprakash, A.E. Hughes, S.P.S. Badwal, Solid State Ionics 121 (1999) 1.
[13] S.P. Jiang, J.P. Zhang, K. Foger, J. Electrochem. Soc. 147 (2000) 3195.
[14] J. Divisek, L.G.J. de Haart, P. Holtappels, T. Lennartz, W. Mallener, U. Stimming, K. Wippermann, J. Power Sources 49 (1994) 257.
[15] J. Mizusaki, H. Tagawa, K. Tsuneyoshi, A. Sawata, J. Electrochem. Soc. 138 (1991) 1867.
[16] V. Brichzin, J. Fleig, H.-U. Habermeier, I. Maier, Electrochem. Solid State Lett. 3 (2000) 403.
[17] M. Kuznecov, P. Otschik, K. Eichler, W. Schaffrath, Ber. Bunseges. Phys. Chem. 102 (1998) 1410.
[18] H. Tsukuda, A. Yamashita, in: U. Bossell (Ed.), Proceedings of the 1st European Solid Oxide Fuel Cell Forum, European Fuel Cells Group, Lucerne, Switzerland, 1994, p. 715.
[19] S.P. Jiang, J.G. Love, Solid State Ionics 138 (2001) 183.
[20] R. Donelson, S. Amarasinghe, D. Goble, D. Hickey, S.P. Jiang, J. Love, T. Quach, in: P. Stevens (Ed.), Proceedings of the 3rd European Solid Oxide Fuel Cell Forum, European Fuel Cells Group, Lucerne, Switzerland, 1998, p. 151.
[21] B.A. Boukamp, Equivalent Circuit (EQUVCRT.PAS) Users Manual, 2nd Edition, Department of Chemical Technology, University of Twente, 1989.
[22] M.J. Verker, M.W.J. Hammink, A.J. Burgraaf, J. Electrochem. Soc. 130 (1983) 78.
[23] S.P. Jiang, S.P.S. Badwal, Solid State Ionics 123 (1999) 209.
[24] T. Kenjo, K. Wada, Solid State Ionics 67 (1994) 249.
[25] Y. Takeda, R. Kanno, M. Noda, Y. Tomida, O. Yamamoto, J. Electrochem. Soc. 134 (1987) 2656.

[26] I. Yasuda, K. Ogasawara, M. Hishinuma, T. Kawada, M. Dokiya, Solid State Ionics 86–88 (1996) 1197.
[27] S.P. Jiang, Solid State Ionics 146 (2002) 1.
[28] F.T. Ciacchi, K.M. Crane, S.P.S. Badwal, Solid State Ionics 73 (1994) 49.
[29] K. Park, D.R. Olander, J. Electrochem. Soc. 138 (1991) 1154.
[30] H. Uchida, M. Yoshida, M. Watanabe, J. Electrochem. Soc. 146 (1999) 1.
[31] G. Chiodelli, M. Scagliotti, Solid State Ionics 73 (1994) 265.
[32] S.P. hang, Z.-P. Zhang, K. Foger, submitted for publication.